



Article

Evaluation and Applicability Analysis of GPM Satellite Precipitation over Mainland China

Xinshun Pan ^{1,2,3,4}, Huan Wu ^{1,2,3,5} , Sirong Chen ^{6,*}, Nergui Nanding ⁷ , Zhijun Huang ^{1,2,3}, Weitian Chen ^{1,2,3}, Chaoqun Li ^{1,2,3} and Xiaomeng Li ^{1,2,3}

- ¹ School of Atmospheric Sciences, Sun Yat-sen University, Zhuhai 519082, China; panxinsh@mail2.sysu.edu.cn (X.P.); wuhuan3@mail.sysu.edu.cn (H.W.); huangzhj5@mail2.sysu.edu.cn (Z.H.); chenwt53@mail2.sysu.edu.cn (W.C.); lichq6@mail2.sysu.edu.cn (C.L.); lixm98@mail2.sysu.edu.cn (X.L.)
- ² Southern Marine Science and Engineering Guangdong Laboratory (Zhuhai), Zhuhai 519082, China
- ³ Guangdong Province Key Laboratory for Climate Change and Natural Disaster Studies, Sun Yat-sen University, Zhuhai 519082, China
- ⁴ Nanhai Meteorological Bureau of Foshan, Foshan 528315, China
- ⁵ Earth System Science Interdisciplinary Center (ESSIC), University of Maryland, College Park, MD 20742, USA
- ⁶ Guangxi Climate Center, Nanning 530022, China
- ⁷ School of Earth Sciences, Yunnan University, Kunming 650500, China; nanding@ynu.edu.cn
- * Correspondence: chensirong@sohu.com; Tel.: +86-13878184004

Abstract: This study aims to systematically evaluate the accuracy and applicability of GPM satellite precipitation products (IMERG-E, IMERG-L, and IMERG-F) with varying time lags at different spatial and temporal scales over mainland China. We use quantitative statistical indicators, including correlation coefficient (CC), root mean square error (RMSE), mean absolute error (MAE), mean daily precipitation, probability of detection (POD), false alarm rate (FAR), bias, and equitable threat score (ETS), based on observations from 2419 national gauge sites. The results show that GPM satellite precipitation products perform well in eastern and southern humid regions of China, with relatively poorer performance in western and northern regions in terms of spatial distribution. It reflects the sensitivity of GPM precipitation retrieval algorithm to climate and precipitation type, topography, density, and quality of ground observation across different latitudes. Despite the design of GPM for different forms of precipitation, IMERG products perform the best in summer and the worst in winter, indicating that estimating snowfalls via satellite is still challenging. In terms of precipitation intensity, IMERG products significantly improve performance for light and no rain ($POD \geq 0.7$), but errors gradually increase for moderate, heavy, and torrential rain, due to the saturation tendency of satellite echoes. Overall, we comprehensively evaluate the IMERG products, revealing the distinct characteristics at various spatial-temporal scales focusing on rainfall accumulations over mainland China. This study provides an important reference for other similar satellite-based precipitation products. It also helps the parameter optimization of hydrological modelling, especially under extreme precipitation conditions, to enhance the accuracy of flood simulation.

Keywords: GPM; IMERG V06; precipitation intensity; satellite precipitation; evaluation; mainland China



Citation: Pan, X.; Wu, H.; Chen, S.; Nanding, N.; Huang, Z.; Chen, W.; Li, C.; Li, X. Evaluation and Applicability Analysis of GPM Satellite Precipitation over Mainland China. *Remote Sens.* **2023**, *15*, 2866. <https://doi.org/10.3390/rs15112866>

Academic Editor: Yongze Song

Received: 2 May 2023

Revised: 26 May 2023

Accepted: 29 May 2023

Published: 31 May 2023



Copyright: © 2023 by the authors. Licensee MDPI, Basel, Switzerland. This article is an open access article distributed under the terms and conditions of the Creative Commons Attribution (CC BY) license (<https://creativecommons.org/licenses/by/4.0/>).

1. Introduction

Precipitation plays a crucial role in the water cycle, e.g., water vapor condenses in the atmosphere and falls to the Earth's surface in the form of rain, snow, sleet, or hail. This process connects atmospheric and surface processes transporting and transmitting matter and energy among global to local atmospheric and hydrological cycles. Understanding of the spatial and temporal distribution of precipitation is very important for various water-related researches and applications, such as water-resource management, agricultural production, drought and flood disaster monitoring, and forecasting [1–4].

Currently, in mainland China, precipitation is monitored mainly using ground-based rain gauges and radar networks. The Chinese meteorological department has deployed more than 60,000 automatic stations nationwide to observe precipitation. There are, currently, more than 270 weather radars in operation in mainland China, with over 110 having undergone dual-polarization technology transformation [5]. However, both observation methods have their limitations, despite the increasing number of rain gauges and the relatively complete radar network deployment in China. Due to the factors such as complex terrain, climate, and human activity, the deployment of ground-based rain gauges and radar stations is still inadequate, with limited numbers and uneven spatial distribution, especially in western China and inland areas where observation facilities are scarce [6]. In addition, there is a high maintenance cost due to the high failure rate of rain gauges. Although rain gauges usually have high accuracy at point locations, various factors, such as complex terrain and temporal and spatial variations in precipitation distribution, highly limit the area representativeness of site-specific precipitation observations [7,8]. The accuracy of radar reflectivity factor Z is affected by multiple factors, including ground clutter, radar-signal attenuation, and variation in vertical profile of reflectivity (VPR), causing errors and uncertainty in precipitation estimation. In addition, the Z–R relationship itself is also influenced by the type of precipitation, which causes quality issues in complex terrain areas and high-altitude regions [9–13]. Therefore, there are remarkable limitations in the spatial coverage and timeliness of current precipitation observations for China merely based on rain gauges and weather radars.

The application of satellite remote sensing can fill the gaps in the above two types of precipitation observations while providing more extensive, continuous, and near-real-time precipitation information. The successful launch and application of the tropical rainfall measuring mission (TRMM) satellite in 1997 marked a new era in global satellite precipitation observation. For the first time, the TRMM satellite carried a Ku-band precipitation radar (PR), which provided three-dimensional distribution information on precipitation intensity. During its 15-year operation, the TRMM satellite significantly improved the accuracy and spatiotemporal resolution of global precipitation observation, playing an important role in studying global climate change and natural disasters [14]. As a follow-up satellite to TRMM, the global precipitation-measurement (GPM) satellite was successfully launched in 2014. The GPM is a national satellite precipitation observation project jointly initiated by NASA and the Japan Aerospace Exploration Agency (JAXA), with the main objective of providing high spatiotemporal resolution and accurate precipitation data for global precipitation monitoring through satellite remote-sensing technology. The GPM satellite alliance includes a core observing satellite (GPM Core Observatory) and multiple other cooperative satellites. The DPR (dual-frequency precipitation radar) and GMI (GPM microwave imager) on board the GPM satellite can provide high-resolution, multi-frequency precipitation observation data worldwide, with more accurate and comprehensive precipitation information for applications in global meteorology, hydrology, water-resources management, and other fields. The DPR is composed of a Ku-band radar (13.6 GHz) and a Ka-band radar (35.5 GHz). The Ku-band radar performs well in detecting moderate to heavy rainfall, while the Ka-band radar, due to its shorter wavelength, is more sensitive to small precipitation particles [15]. The GMI can obtain microwave radiation information in the atmosphere. Through the synergistic effect of these two instruments, the GPM is expected to provide more accurate precipitation observation both for rain and snow with higher time frequency (up to 30 min) from pole to pole. The utilization of GPM satellite products as input parameters in environmental modeling is of great importance, particularly in data-scarce areas. For instance, a recent study integrated GPM precipitation data with the weather research and forecasting (WRF) model to enable early warning and monitoring of flash floods [16]. Moreover, GPM data were useful in the rainfall erosivity estimation based on the widely used RUSLE approach [17] and sustainable water-resources management [18].

However, satellite remote-sensing precipitation-measurement technology is an indirect inversion technology that detects the characteristics of clouds and precipitation through

remote-sensing satellites. Before using satellite remote-sensing precipitation products, their accuracy and reliability must be evaluated at multi-temporal and spatial scales for better understanding the temporal and spatial distribution characteristics of errors. Such evaluation studies can provide important knowledge for the subsequent development of next-generation satellite precipitation products for better hydrometeorological applications. GPM IMERG products have been widely evaluated by various researchers with different evaluation indicators and statistical methods [19–22]. However, previous studies are mostly reported for different geographical regions. There is a lacking of systematic evaluation of its quality over the China against the ground observations. Moreover, studies have indicated that the impact of climate characteristics and terrain on satellite precipitation products varies across different regions with lower accuracy in mountainous and desert regions due to surface reflectance and cloud obstruction. In monsoon regions, the large variation in precipitation also leads to lower accuracy of satellite precipitation products, which requires the combination of various satellite precipitation products and ground-observation data to improve accuracy. Therefore, suitable satellite precipitation products should be chosen based on regional characteristics and demands, and combined with ground-observation data for calibration and optimization in practical applications [23–34].

There are some studies that have evaluated IMERG products over mainland China. Nevertheless, these studies are constrained by limitations, including short data durations and a lack of analysis at the hourly scale [35–38]. In this study, utilizing rain-gauge data from 2419 national meteorological stations from June 2014 to December 2020, we systematically evaluate the accuracy and reliability of the mainstream product IMERG, provided by the GPM satellite, at different temporal and spatial scales, as well as different precipitation intensities, by utilizing rain-gauge data from 2419 national meteorological stations spanning the period from June 2014 to December 2020. Furthermore, the quality assessment revealed the performance differences of IMERG precipitation products between daytime and nighttime at an hourly scale. We seek deeper insights into the patterns and mechanisms of global precipitation changes, and enhance our ability to forecast extreme weather events for better preparation for hydrometeorological hazards, such as floods, droughts, and landslides. This research would also hold a promise for providing valuable feedbacks for the development of future satellite remote-sensing precipitation-measurement technology.

2. Datasets and Methodology

2.1. Study Area

Mainland China is located in the eastern part of Asia and the western coast of the Pacific Ocean (18°N~53°N, 73°E~135°E), with a total land area of approximately 9.6 million square kilometers. It spans temperate, subtropical, and tropical regions from north to south, ranging from Mohe, located at the heart of Heilongjiang River in the north, to Zengmu Ansha of the Nansha Islands in the south. The vast territory of China boasts diverse topography and climate types, featuring a step-like distribution of high west and low east, including the Qinghai-Tibet Plateau, the North China Plain, and the Southeast Hills and Plains. China has a rich variety of climate types, including tropical, subtropical, temperate, and frigid zones. The climate in the eastern coastal regions is warm and humid, while that in the northwest is dry and cold. The Qinghai-Tibet Plateau exhibits characteristics such as high altitude, low oxygen levels, and low atmospheric pressure. Due to the interaction between terrain and monsoon, the distribution of precipitation in China shows more in the east and south, and less in the west and north.

2.2. Data Collection and Processing

2.2.1. The GPM IMERG Precipitation Data

This study utilizes the level-three fusion precipitation product IMERG (integrated multi-satellite retrievals for GPM) provided by the NASA precipitation-measurement program via the website <https://gpm.nasa.gov/GPM> (accessed on 15 June 2022). The IMERG

precipitation products are generated by fusing DPR and GMI data to generate CORRA-G product, which is then matched and calibrated with other microwave data (PMW) from the GPM satellite constellation, further calibrated with geosynchronous orbiting infrared data (IR), and, finally, obtains the comprehensive inversion precipitation data IMERG [39]. Specifically, we use the IMERG V06 version of precipitation products from June 2014 to December 2020, including IMERG-E (early), IMERG-L (late), and IMERG-F (final).

Compared with other satellite precipitation products, IMERG has a wider coverage area, including the polar regions, and higher spatiotemporal resolution, providing precipitation datasets with different lag times [25]. For instance, IMERG-E is released earliest, providing global near-real-time precipitation data with a time lag of about four hours. This product uses GPM core satellite-observation data and other satellite data, combined with pre-correction based on ground-based precipitation-measurement data, to generate satellite precipitation-estimation results. It aims to provide timely precipitation estimation for monitoring and prediction in a short period of time. IMERG-L is developed based on IMERG-E, using more observation data for calibration, including multiple satellite radar data and other satellite information, improving the accuracy and spatial resolution of precipitation estimation, but with a time lag of about 12 h. IMERG-F is the final precipitation product set which integrates all available data sources in the calibration process, including all GPM core satellite-observation data, multiple satellite radar and microwave radiometer data, and ground-based observation data. The lag time of IMERG-F is about three months.

2.2.2. Rain Gauge

This study utilized rain-gauge data from 2419 national meteorological stations from June 2014 to December 2020, as shown in Figure 1. The temporal resolution of the data was one hour, with the precipitation resolution of 0.1 mm, and all meteorological data underwent strict quality control with minimal missing data. After removing missing and a small number of abnormal values through quality-control procedures, a total of 2418 stations were obtained. Hourly precipitation data were cumulated to obtain the required precipitation data for every three hours and daily, respectively, resulting in 44,399,957 (accounting for 95.36%) and 5,581,328 data samples (accounting for 95.90%).

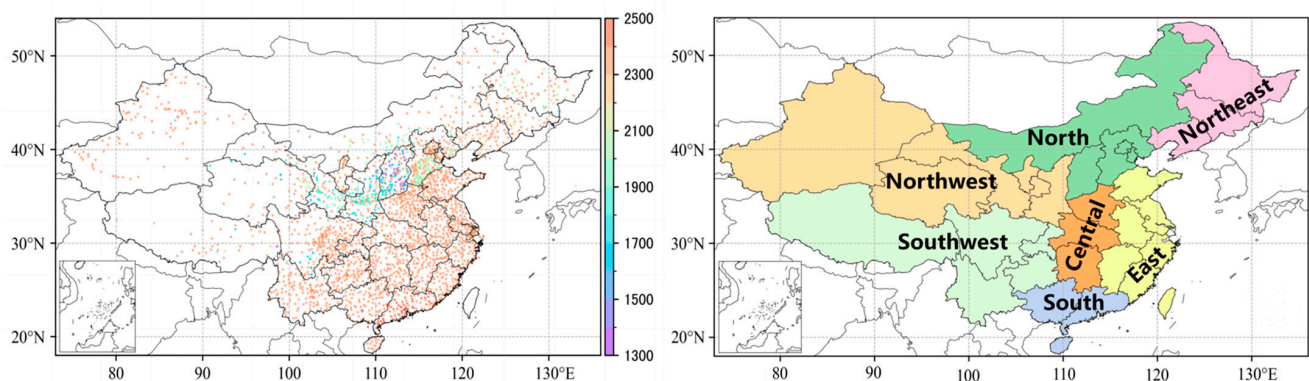


Figure 1. Map of the study area containing the distribution of national meteorological stations (points) and the number of data samples for each station (**left panel**), and spatial distribution of the seven sub-regions over mainland China (**right panel**).

2.2.3. Data Preprocessing

The V06 version of IMERG data is in grid format, while the national surface meteorological observation station data are in site format. Moreover, these two types of measurements have different temporal and spatial resolutions. Therefore, to evaluate the accuracy and applicability of IMERG precipitation products, it is necessary to pre-process the IMERG data for comparison with observation data. For IMERG precipitation products, at a time scale, data at 00 min and 30 min are added to obtain precipitation data for every three hours and daily accumulations (00:00–00:00 UTC, same for the following); at a spatial

resolution, due to the vast range of China and the uneven distribution of stations, the accumulated precipitation data for every three hours and daily are interpolated to the corresponding location of ground stations using bilinear interpolation method (this article does not consider the possible errors caused by bilinear interpolation). For ground observations, at a time scale, precipitation data for each hour are cumulated to obtain three-hourly and daily accumulations, without any processing at spatial scale. This provides corresponding precipitation data for IMERG products and gauge observations for every three hours and daily in mainland China. Based on this data, an evaluation of the accuracy and applicability of GPM precipitation products in mainland China will follow.

2.3. Evaluation Techniques

This study utilized two types of evaluation indicators: statistical indicators and detection indicators. By comparing satellite precipitation data with gauge observations and assessing its detection ability at different precipitation intensities, a comprehensive analysis of the accuracy of GPM IMERG precipitation products was conducted.

2.3.1. Statistical Indicators

In terms of statistical indicators, this study employed several commonly used metrics, such as Pearson's correlation coefficient (CC), root mean square error (RMSE), mean absolute error (MAE), and average daily precipitation to quantitatively evaluate the correlation and degree of deviation of IMERG precipitation products. Specifically, CC was used to measure the linear correlation between satellite precipitation data and ground automatic station observation data; RMSE reflects the difference between the satellite observation data sequence and the actual observation value and is used to evaluate the overall error level of satellite precipitation products; MAE represents the average absolute deviation degree between satellite precipitation data and station observation data, which evaluates the deviation trend of IMERG products and ground rainfall stations as a whole. Average daily precipitation is defined as the cumulative precipitation divided by the total sample days at a given time period. Through the comprehensive application of these indicators, this study conducted an in-depth analysis on the accuracy and applicability of GPM IMERG precipitation products.

$$CC = \frac{\sum_{i=1}^N (P_i - \bar{P})(S_i - \bar{S})}{\sqrt{\sum_{i=1}^N (P_i - \bar{P})^2 (S_i - \bar{S})^2}} \quad (1)$$

$$RMSE = \sqrt{\frac{\sum_{i=1}^N ((P_i - S_i)^2)}{N}} \quad (2)$$

$$MAE = \frac{1}{N} \left| \sum_{i=1}^N (P_i - S_i) \right| \quad (3)$$

where P_i is the value of GPM IMERG products rainfall and \bar{P} is the mean of P_i , S_i is the value of ground rainfall stations, and \bar{S} is the mean of S_i , and N is the total number of data records.

2.3.2. Detection Indicators

Detection indicators include the probability of detection (POD), false-alarm rate (FAR), bias, threat score (TS), and the equitable threat score (ETS). These are used to evaluate the IMERG precipitation product's ability to capture precipitation events [40].

These indicators are widely used in comparative studies between observation stations and satellite retrieval products. Among them, POD represents the probability that actual rainfall is correctly detected by GPM satellites. A higher POD value indicates a lower rate of missed precipitation events by satellite precipitation products. FAR reflects the false-alarm rate of satellite data for precipitation events. Bias describes the virtual report (bias > 1) and missed report (bias < 1) conditions of satellite data relative to observation data to evaluate

the systematic bias in satellite precipitation product. ETS measures the comprehensive detection accuracy of satellite data for actual rainfall under random circumstances in different time and space. Higher TS and ETS scores indicate stronger comprehensive prediction capabilities of satellite precipitation products for precipitation events.

This study referred to the national standard “Precipitation Intensity Classification” (GB/T28592-2012) (National Meteorological Center, 2012) and divided precipitation intensity into five categories based on 24 h precipitation amount: no rain, light rain, moderate rain, heavy rain, and torrential rain or above, with corresponding precipitation amounts of (0, 0.1), (0.1, 10), (10, 25), (25, 50), and (50, ∞) mm/24 h, respectively. Then, based on the range of these precipitation intensities, these indicators were quantitatively analyzed in a graded manner. Through these categorized indicators, the capture ability of IMERG precipitation products for different precipitation levels can be evaluated.

$$POD = \frac{Hits}{Hits + Misses} \quad (4)$$

$$FAR = \frac{False_alarms}{Hits + False_alarms} \quad (5)$$

$$BIAS = \frac{Hits + False_alarms}{Hits + Misses} \quad (6)$$

$$TS = \frac{Hits}{Hits + Misses + False_alarms} \quad (7)$$

$$ETS = \frac{Hits - Hit_random}{Hits + Misses + False_alarms - Hit_random} \quad (8)$$

$$where\ Hit_random = \frac{(Hits + Misses)(Hits + False_alarms)}{Total} \quad (9)$$

In the equation, *Hits* represents the number of times GPM precipitation products and ground precipitation sensors exceeded the threshold; *False alarms* indicate the number of times GPM precipitation products exceeded the threshold, but ground precipitation sensors were below the threshold; *Misses* refers to the number of times GPM precipitation products were below the threshold, but ground precipitation sensors exceeded the threshold; *False random* represents the number of times GPM precipitation products randomly hit.

3. Results and Discussion

The complex terrain and diverse climate in mainland China pose high requirements for satellite precipitation products. Accuracy assessment is helpful to gain a deeper understanding of the performance and reliability of IMERG precipitation products in mainland China. Through accuracy assessment, we can discover errors and deficiencies in IMERG in mainland China and adopt appropriate calibration and fusion methods to improve data quality. For example, incorporating ground-observation data, other satellite precipitation products, or auxiliary information (such as soil moisture, vegetation index, etc.) into the fusion and calibration process can improve the accuracy of precipitation data [41,42]. Based on the accuracy assessment, IMERG precipitation products or IMERG-based correction products can also be applied in hydrological modeling fields, such as flood forecasting and runoff simulation [43].

3.1. Analysis of IMERG Precipitation Product Accuracy

3.1.1. Overall Rainfall Accuracy Analysis

We used data from 2418 national meteorological observation stations across China from June 2014 to December 2020 as independent variables and conducted linear regression analysis using three IMERG datasets as dependent variables (Table 1). It can be seen that

the CC values of all IMERG products with respect to observed values are greater than 0.67, RMSE is greater than 6.31 mm/d, MAE is greater than 2.30 mm/d, and RE is greater than 17.8%. This indicates that GPM data has high correlation ($CC \geq 0.67$) and consistency with measured data overall, but there is a certain degree of deviation and overestimation.

Table 1. Overall evaluation indices of GPM satellite daily precipitation products IMERG-E, IMERG-L, and IMERG-F.

	CC	RMSE (mm/d)	MAE (mm/d)	RE (%)
IMERG-E	0.67	7.03	2.53	20.1
IMERG-L	0.69	7.01	2.44	21.1
IMERG-F	0.74	6.31	2.30	17.8

In mainland China, IMERG precipitation products and ground observations show a generally high correlation (Figure 2). The performance of the IMERG product datasets is as follows: IMERG-E < IMERG-L < IMERG-F, with correlation coefficients of 0.67, 0.69, and 0.74, respectively. It can be seen that the slope of the fitted line of the IMERG product to the observations is less than 1, indicating an overestimation by the IMERG products. This may be caused by errors in satellite-retrieved raindrops due to evaporation during the falling process and errors in rainfall records by meteorological observation stations. Overall, the data collected by IMERG-E and IMERG-L have similar performances, while the data from IMERG-F are more concentrated, indicating better accuracy. Additionally, for heavy rain or above, the scatter distributions of the IMERG products are more concentrated in the upper half, indicating a trend of underestimation of actual rainfall by IMERG product in the case of heavy rainfall or above. This may be because the frequency of extreme precipitation events is low, leading to insufficient inversion capabilities of GPM satellite products for extreme precipitation events. Nevertheless, the correlation coefficient of IMERG-F is still the highest, with correlation coefficients of IMERG-E, IMERG-L, and IMERG-F being 0.39, 0.41, and 0.47, respectively.

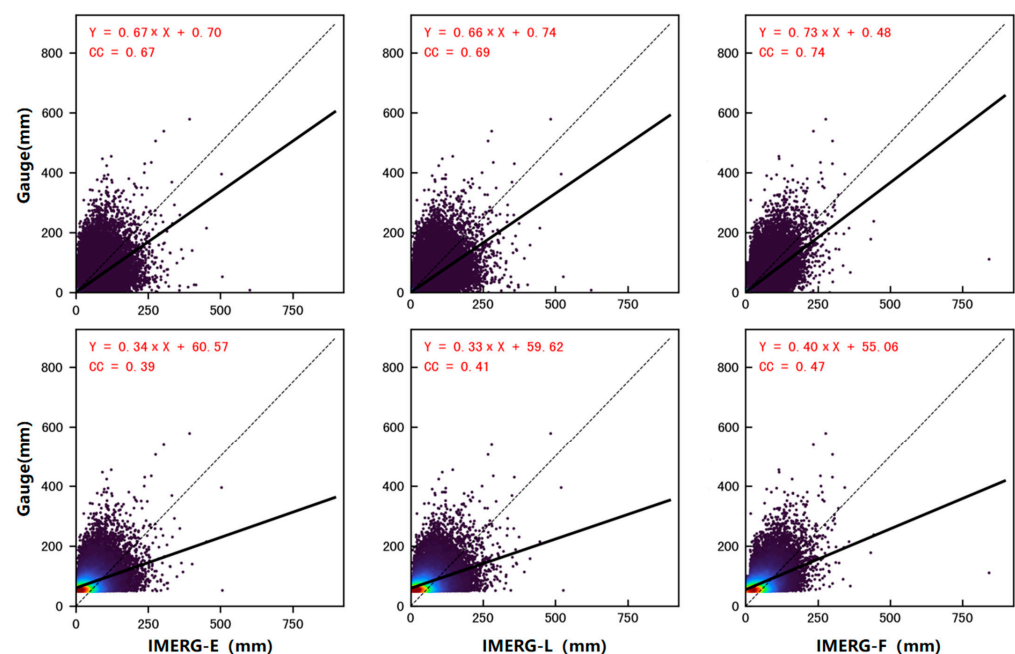


Figure 2. Scatter plot and linear regression curve of gauge-GPM IMERG products, with the horizontal axis representing the values of GPM IMERG products rainfall and the vertical axis representing value of ground rainfall stations (the color intensity represents data density).

3.1.2. Accuracy Analysis in Different Regions of China

In most parts of mainland China, there is a high correlation between IMERG product and ground observations. Among them, the correlation in the eastern region is higher than that in the western region (Figure 3). Nationally, the proportions of sites with daily precipitation correlation coefficients greater than 0.6 is 84.4%, 90.0%, and 95.9% for IMERG-E, IMERG-L, and IMERG-F, respectively, while the proportion of sites with coefficients greater than 0.7 is 21.6%, 36.4%, and 73.0%, respectively. This indicates that the correlation coefficient between GPM precipitation products and observation data are generally above 0.6, and the correlation coefficient of IMERG-F is generally above 0.7, with a higher proportion of sites with values above 0.7 compared to the other two products, indicating that the data quality of IMERG-F is better than that of IMERG-E and IMERG-L.

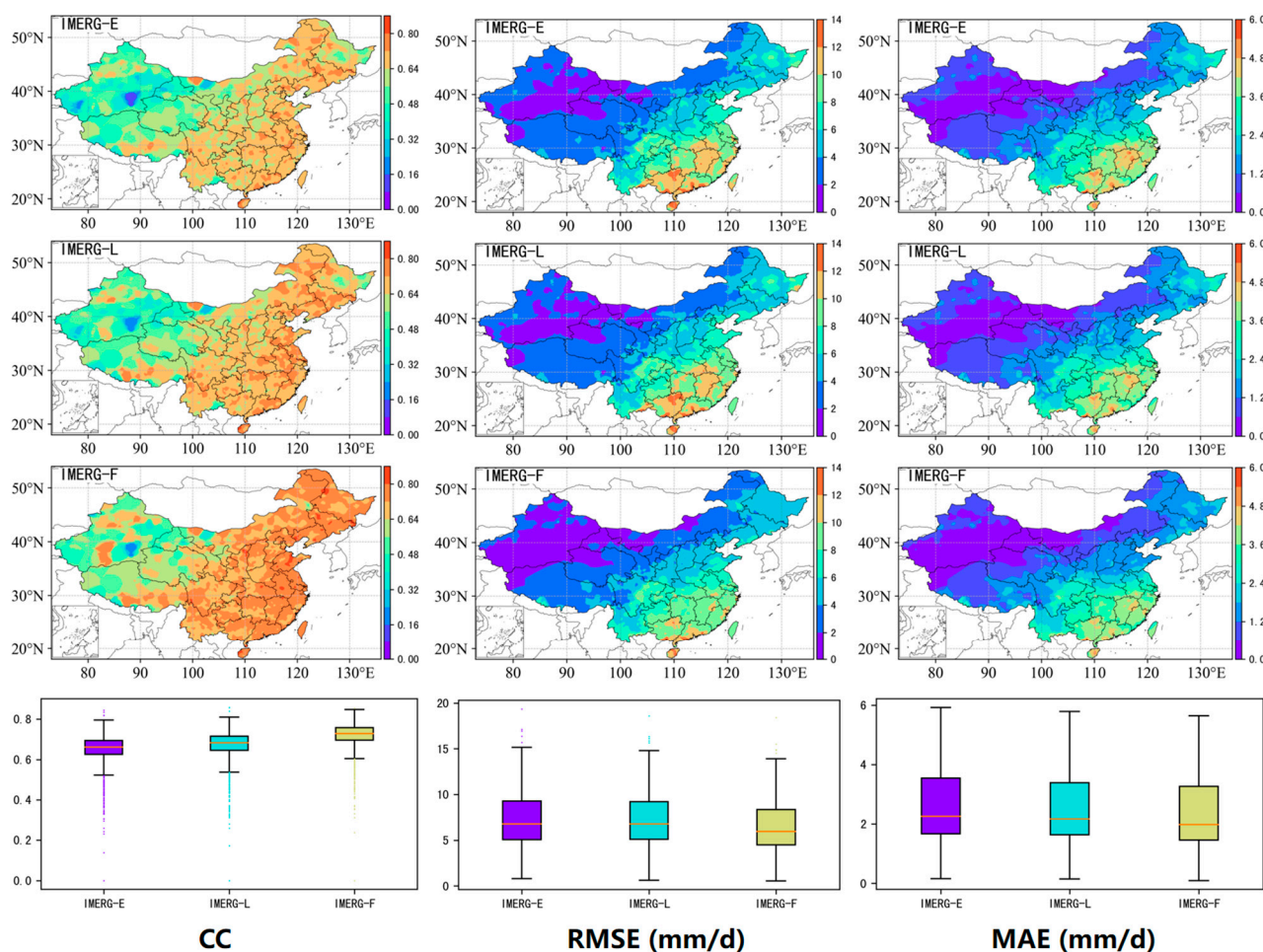


Figure 3. Spatial distribution of various indices for GPM IMERG products, with CC, RMSE, and MAE displayed from left to right, and IMERG-E, IMERG-L, and IMERG-F with corresponding boxplots arranged from top to bottom. In the boxplots, the five horizontal lines from top to bottom represent the maximum value, upper quartile, median, lower quartile, and minimum value, respectively. Dots outside the maximum and minimum values are considered as outliers.

As shown in boxplots in Figure 3, the median CC of IMERG-F is clearly higher than that of IMERG-E and IMERG-L, and the data distribution is more concentrated, indicating that the correlation performance of IMERG-F is superior to the other two products. However, all three products have some outliers. Correlation coefficients at some stations are less than 0.4, indicating poor performance of IMERG products at those sites. These sites, mainly distributed in the western region, can be influenced by factors such as terrain complexity, climate characteristics, data quality, instrument calibration, and atmospheric conditions.

From the spatial distribution and boxplots of RMSE and MAE, the GPM IMERG products show similar distribution patterns. RMSE is mostly concentrated in 5–10 mm/d, with some large outliers; MAE is mostly concentrated in 1.8–2.8 mm/d, without obvious outliers. The errors of GPM precipitation products decrease step by step from the southeast coastal region to the northwest inland region. In the southeast and southern China regions, the error values are generally high, with RMSE mainly distributed above 8.5 mm/d and 9.5 mm/d, and MAE mainly distributed above 3 mm/d and 3.5 mm/d, respectively. Conversely, the error values in the Northwest and Inner Mongolia regions are relatively low, with average RMSEs below 2.5 mm/d and 5.5 mm/d, and average MAEs below 0.8 mm/d and 1.5 mm/d, respectively.

In summary, the correlation is better in the southeastern and southern China regions, but the overall error is higher, while the correlation is lower in the Northwest and Inner Mongolia regions, but the error is smaller. In addition, the error in most regions of the country is positive, indicating an overestimation of observed rainfall by IMERG products. IMERG-F shows the same trend as the other two products in terms of different indicators and regions, but its performance is relatively better. The spatial variability of errors in precipitation estimation in China can be attributed to various factors. Complex terrain presents challenges for satellite remote sensing, resulting in higher errors. Regions with sparse or unreliable meteorological stations lack accurate ground truth data, leading to increased errors. Sporadic and intense precipitation events in certain areas pose difficulties for accurate estimation using remote sensing. Additionally, factors such as seasonality, precipitation patterns, land-use changes, and anthropogenic influences also contribute to the spatial variability of errors in precipitation estimation across China.

3.1.3. Accuracy Analysis of Different Altitudes in China

The correlation coefficient between IMERG products and observations gradually decreases as the altitude increases, with a CC value ranging from 0.57 to 0.73 (Figure 4). For different altitude intervals, the order of the correlations between three IMERG products and observations remains the same: IMERG-F > IMERG-L > IMERG-E. As altitude increases, the errors gradually decrease, with RMSE ranging from 2.9–7.8 mm/d and MAE ranging from 1.1–2.8 mm/d. In low-altitude areas (<2000 m), IMERG products have the best correlation with actual precipitation compared to the other altitudes, but the errors are relatively large. Among them, IMERG-F product performs better than the other two products in both correlation and errors, with an average correlation coefficient of 0.72, RMSE of 6.50 mm/d, and MAE of 2.36 mm/d; while IMERG-E performs the worst, with an average correlation coefficient of 0.65, RMSE of 7.27 mm/d, and MAE of 2.61 mm/d.

In mid-altitude areas (2000–4000 m), the correlations between IMERG products and observations decrease dramatically compared to low-altitude areas. Among them, IMERG-F still performs the best, with a correlation coefficient of 0.68, while IMERG-E performs the worst, with a correlation coefficient of 0.61. The bias of IMERG products decreases relative to low-altitude areas, with similar RMSE and MAE performance, with values around 3.75 mm/d and 1.4 mm/d. In high-altitude areas (>4000 m), the correlation coefficient of IMERG precipitation products further decreases. Although IMERG-F still has an advantage in terms of correlation, it has the largest decrease in correlation, and its bias reduction trend slows down, with the bias higher than the other two products, indicating that IMERG-F performs relatively poorly in high-altitude areas. This can be attributed to various factors, including the intricate topography, calibration biases, limited data coverage, difficulties in satellite-based retrievals, and the unique atmospheric dynamics present in high-altitude regions. These factors contribute to discrepancies between observations and IMERG products, thereby impacting the performance of IMERG-F. The RMSE and MAE of IMERG-F show higher values in high-altitude regions. These elevated values can be attributed to the limited ground-based observation networks used for the bias correction process in final product, which may lead to higher errors. Moreover, the limited number of gauges used in this quality assessment can also bias the result. In terms of daily rainfall, IMERG

products show overestimation of precipitation in low-altitude areas, which may be due to the fact that the precipitation detected by the GPM satellite is mainly at high altitude in the atmosphere, and some precipitation may evaporate during the landing process, resulting in actual precipitation being smaller than satellite precipitation. In mid-to-high-altitude areas, IMERG products show different trends: IMERG-F overestimates precipitation, while IMERG-E and IMERG-L underestimate the observations. This difference may be due to the effect of snow cover in mid- to high-altitude areas, which causes changes in satellite observation accuracy, while IMERG-F is affected by rain gauge data added for quality control in the later stage, and the average daily rainfall performance is closer to the actual situation.

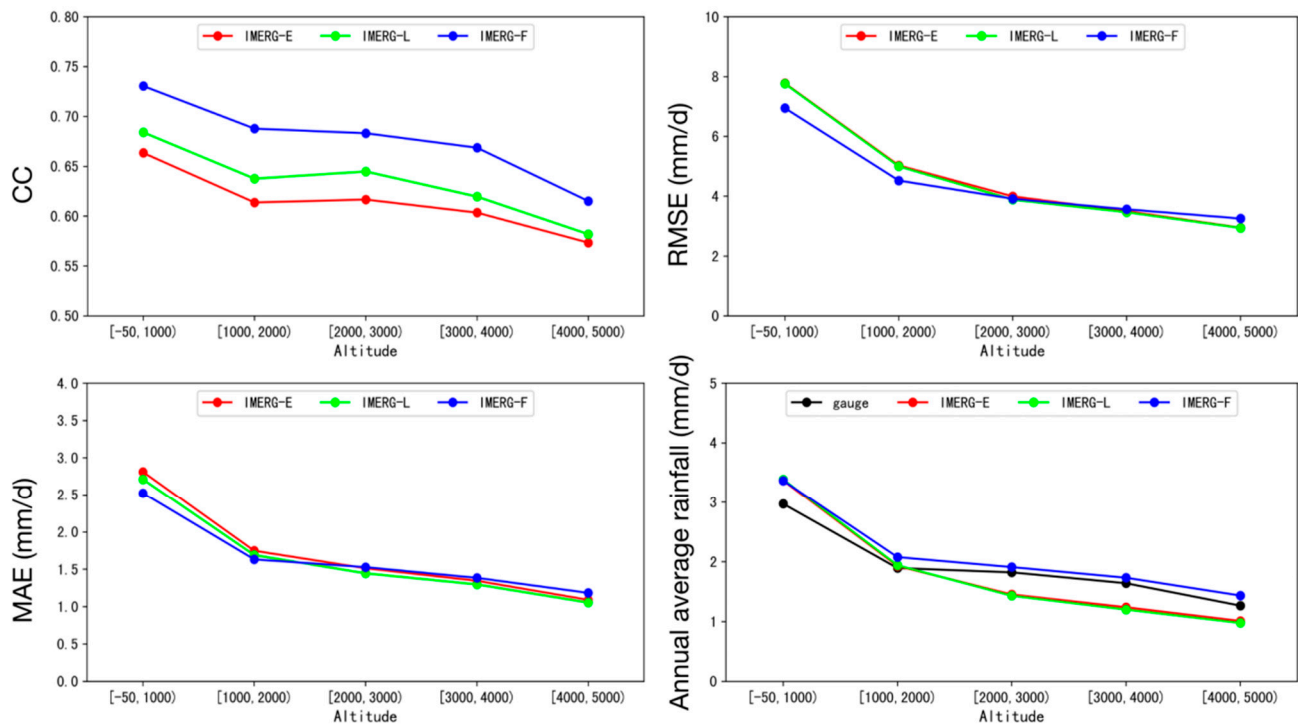


Figure 4. Comparison of GPM satellite products IMERG-E, IMERG-L, and IMERG-F at different altitude bands in terms of CC, RMSE, MAE, and annual average daily precipitation.

In summary, IMERG satellite products have higher applicability in mid-altitude areas, while there are certain errors in low-altitude and high-altitude areas, which need to be further corrected. For example, in low-altitude areas, local ground observation data can be combined to calibrate IMERG precipitation products to improve their accuracy. In high-altitude areas, other remote-sensing data sources can be used or specific corrections can be made to satellite products to reduce errors.

3.2. Accuracy Analysis at Different Time Scales

3.2.1. Annual Accuracy Analysis

Overall, precipitation in mainland China gradually decreases from southeast to northwest (Figure 5). The southeastern and south parts of China have the highest amount of precipitation, with average daily rainfall of 4.67 mm/d and 4.27 mm/d, respectively, and, in some areas, it even exceeds 7 mm/d. In contrast, the average daily rainfall in the northwest, Inner Mongolia, and northeastern regions is less than 2 mm/d, with values of 0.51 mm/d, 1.41 mm/d, and 1.72 mm/d, respectively.

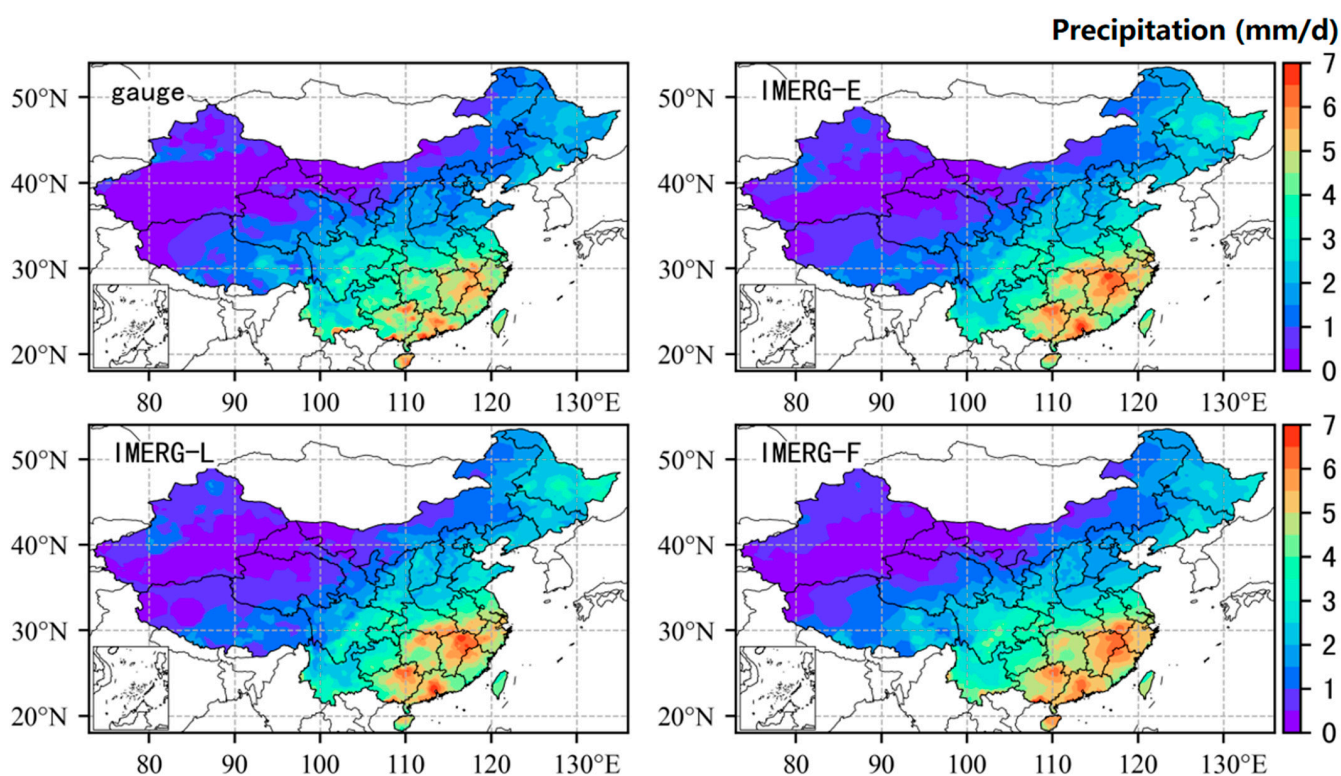


Figure 5. Spatial distribution of average daily precipitation for mainland China estimated by gauge stations and GPM satellite products IMERG-E, IMERG-L, and IMERG-F (June 2014 to December 2020).

IMERG precipitation products are generally consistent with ground observations in terms of spatial distribution of average daily rainfall, indicating that GPM satellite-inverted rainfall can reflect the overall precipitation spatial characteristics of mainland China well. However, there are certain errors in the average daily rainfall estimated by IMERG precipitation products. In areas with more precipitation (average daily rainfall exceeding 3 mm), IMERG products can better reflect the location and intensity of precipitation centers, but, overall, they tend to overestimate the spatial extent and intensity of precipitation, such as in the southern region and the Yangtze River Basin. In terms of details, IMERG still has some shortcomings. For example, IMERG could not accurately reflect the three major rainstorm centers in Guangdong, and there was an underestimation of rainstorm centers along the coast of eastern and western Guangdong. This may be related to the dynamic and thermal mechanisms of precipitation in the coastal areas of Guangdong, especially considering the underestimation of precipitation by IMERG under low-altitude jet stream background [32]. In areas with less precipitation (daily average rainfall below 3 mm), IMERG products perform well. However, there are still large errors in the northeastern region, which may be related to the rain belt moving northward during July and August. Compared with the other two products, IMERG-F can more accurately reflect the distribution of precipitation in China. For example, in the map of IMERG-F average daily rainfall, the three major rainstorm centers in Guangdong are clearly visible, while the other two products can only show two rainstorm centers and fail to replicate the rainstorm center along the coast of eastern Guangdong.

Therefore, although GPM satellite products can well reflect the precipitation characteristics of mainland China in terms of spatial distribution, there are still certain errors in some details and areas. In order to improve the accuracy of precipitation estimation, IMERG products can be further calibrated and optimized, especially for areas with more precipitation, such as the southern, southeastern, and northeastern regions of China.

3.2.2. Accuracy Analysis at Different Seasons

In terms of the seasonality in correlation coefficients (Figure 6), IMERG precipitation products show good consistency with observations in the months from April to October, with correlation coefficients of 0.65, 0.67, and 0.70 for IMERG-E, IMERG-L, and IMERG-F, respectively. The performance in other months is generally lower, with correlation values of 0.49, 0.51, and 0.57, respectively. The highest correlation coefficient appears in May (IMERG-F, 0.72), while the lowest appears in January (IMERG-E, 0.41). Looking at different seasons, all IMERG products perform poorly in winter, with correlation coefficients ranging between 0.45 and 0.52. This may be related to the dryness and low rainfall in winter. In spring and autumn, the correlation coefficients rise above 0.6, showing better consistency with observed rainfall. In summer, the correlation coefficient reaches its peak, exceeding 0.65, with the strongest correlation. Overall, the trends of RMSE and MAE of IMERG products are similar across the country. In the wet season, RMSE and MAE reach their peaks. Across the country, the RMSE and MAE peaks move northward along with China's main rain belt. The highest RMSE and MAE for IMERG-E and IMERG-L mainly occur in June and July, with maximum values of 1.8 mm/d and 1.36 mm/d, respectively. However, IMERG-F shows some delay, with peaks mainly occurring in July, and the maximum values of RMSE and MAE reduce to 1.17 mm/d and 0.9 mm/d, respectively. During winter months, the values are lower, with the lowest points occurring in December, and RMSE and MAE are both below 0.24 mm/d and 0.15 mm/d, respectively. The monthly variation of RMSE and MAE is very similar to the monthly precipitation change observed by ground stations, indicating that RMSE and MAE are positively correlated with monthly precipitation.

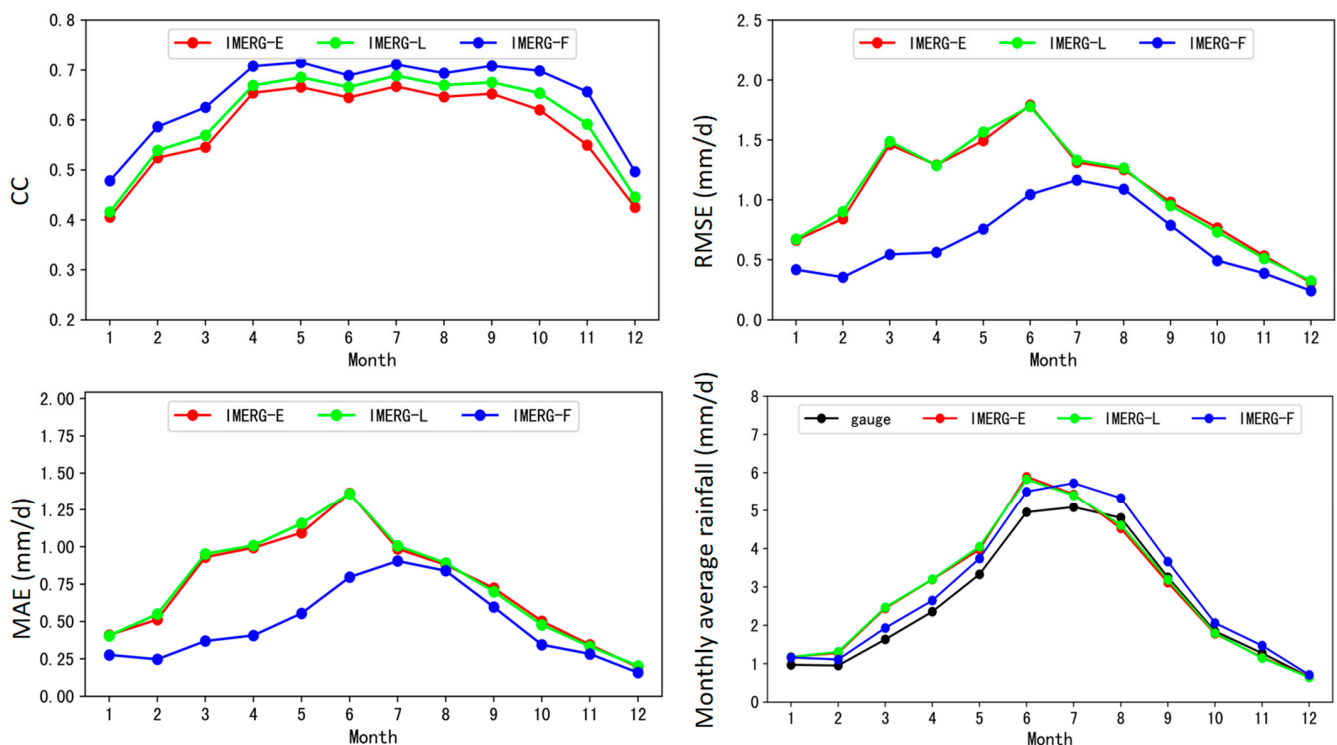


Figure 6. Performance indices based on monthly average daily rainfall for IMERG-E, IMERG-L, and IMERG-F (correlation coefficient, RMSE, MAE, and difference between IMERG and observed monthly average daily precipitation).

IMERG-E and IMERG-F precipitation show overestimation in the first half of the year and underestimation in the second half of the year on the month-to-month average daily rainfall. Looking at the seasons, precipitation estimation in winter is better, while precipitation in spring is significantly overestimated. There are fluctuations in summer, with overestimation in early summer and underestimation in late summer, while precipitation

in autumn is significantly underestimated. This seasonal variation may be due to the relatively high rainfall in summer, leading to an increase of errors in the GPM satellite precipitation product.

In conclusion, IMERG satellite products show good consistency with ground observation from April to October, but performance in other months is generally poorer. The large amount of rainfall in summer leads to an increase in errors in the GPM precipitation products. In addition, based on the month-to-month average daily rainfall, IMERG-E and IMERG-F overestimate actual precipitation in the first half of the year and underestimate it in the second half of the year. These results have important implications for further research and improvement of the accuracy of GPM satellite products in different seasons and regions.

3.2.3. Spatial Distribution of Seasonal Average Daily Precipitation

IMERG products can generally estimate the precipitation distribution in China well for each season (Figure 7). However, for the Yangtze River Basin and southern China, errors in spring and summer are relatively large, mainly manifested as overestimation of spatial extent and intensity. This error may be related to the seasonal northward movement of rain belts affected by the weather-scale circulation such as monsoon outbreak and the northward movement of subtropical high pressure. In addition, IMERG tends to underestimate extreme precipitation, which may be due to a lack of extreme precipitation samples in the GPM satellite's precipitation algorithm. In the Northeast region, there is a large estimation error in spring and summer precipitation, which may be due to a joint effect of frequent cold air activity in Northwest China and warm and humid airflow over the Sea of Japan. In autumn, IMERG-E and IMERG-L have large errors on Hainan Island, which may be related to the long-term hovering of the tropical convergence zone near Hainan Island. Among all products, IMERG-F has the best performance in precipitation estimation, while the other two products have relatively large errors.

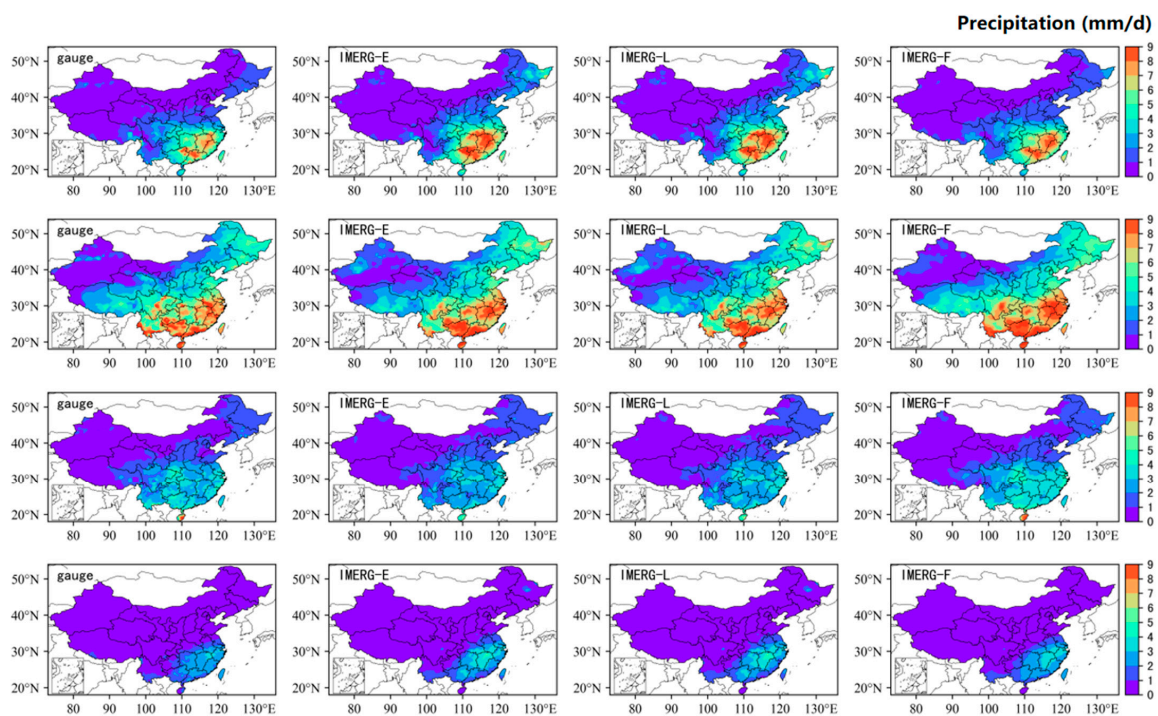


Figure 7. Spatial distribution of seasonal average daily precipitation for IMERG products and gauge observations, with IMERG-E, IMERG-L, and IMERG-F displayed from left to right, and spring, summer, autumn, and winter arranged from top to bottom.

Therefore, although IMERG products have some errors in estimating precipitation in China, these data still have high reference value. By analyzing the errors in each season in depth, valuable insights can be provided for improving the accuracy of GPM satellite products in different seasons and regions.

3.3. Hourly Accuracy Analysis

3.3.1. Spatial Distribution of Average Hourly Rainfall

Daily precipitation data can reflect the characteristics of precipitation changes in China to a certain extent, but its temporal resolution cannot meet the needs of short-term forecasts, hydrological monitoring, and daily business operations. Therefore, studying the quality of satellite precipitation products at hourly timescale has important practical value for meeting these needs.

Figure 8 analyzes the spatial distribution of the average rainfall at three-hourly timescale in mainland China from June 2014 to December 2020 estimated by gauge stations and GPM IMERG satellite products. The results show that there are two precipitation peaks in mainland China: the first peak appears between 21:00–00:00 (UTC, equivalent to 05:00–08:00 CST, China Standard Time) (Figure 9), and the maximum precipitation zone mainly located in southern and southeastern China; the second peak appears between 06:00–09:00 (UTC, equivalent to 14:00–17:00 CST) (Figure 9), and the maximum precipitation zone is located along the coast, especially near the Guangdong coast and Hainan Island. Compared with observation data, GPM satellite products can reflect the overall trend of three-hourly precipitation change in mainland China more accurately, but there is still a significant deficiency in identifying heavy precipitation events.

For the average hourly rainfall in areas with higher precipitation in China such as southern and southeastern China and Hainan Island, IMERG precipitation products show a certain degree of overestimation. Comparing the three IMERG products, it is found that they can better reflect China's precipitation changes. Specifically, IMERG-F performs better than IMERG-E and IMERG-L overall, with a significant improvement in identifying precipitation center and intensity, which indicates that the performance of IMERG-F has been significantly improved after gauge correction.

3.3.2. Analysis of Hourly Average Rainfall Accuracy

From the distribution characteristics of the correlation coefficient at three-hourly timescale in the national scope (Figure 9), the correlation coefficient between IMERG precipitation products and observed rainfall shows a bimodal feature over time, with good performance observed between 18:00–03:00 and 12:00–15:00 (UTC, same as following), with the correlation coefficient ranging between 0.50 and 0.55. The correlation coefficients for other periods are generally lower, but not less than 0.4, ranging from 0.41 to 0.48. This indicates that the performance of GPM satellite products is acceptable at the hourly scale, with the highest correlation coefficient appearing between 21:00–00:00 and 00:00–03:00 (0.55 for IMERG-F) and the lowest appearing between 09:00–12:00 (0.41 for IMERG-L). The RMSE and MAE of IMERG products exhibit a similar bimodal distribution pattern, with the minimum values of both occurring between 00:00–03:00, with values lower than 0.09 mm/3 h and 0.07 mm/3 h, respectively. The maximum value of RMSE and MAE occurs between 15:00–18:00 h, which is 0.13 mm/3 h and 0.1 mm/3 h (IMERG-L), respectively. The trend, peak, and valley positions of RMSE and MAE are generally in line with the distribution of three-hourly average rainfall, while the correlation coefficient shows the opposite trend.

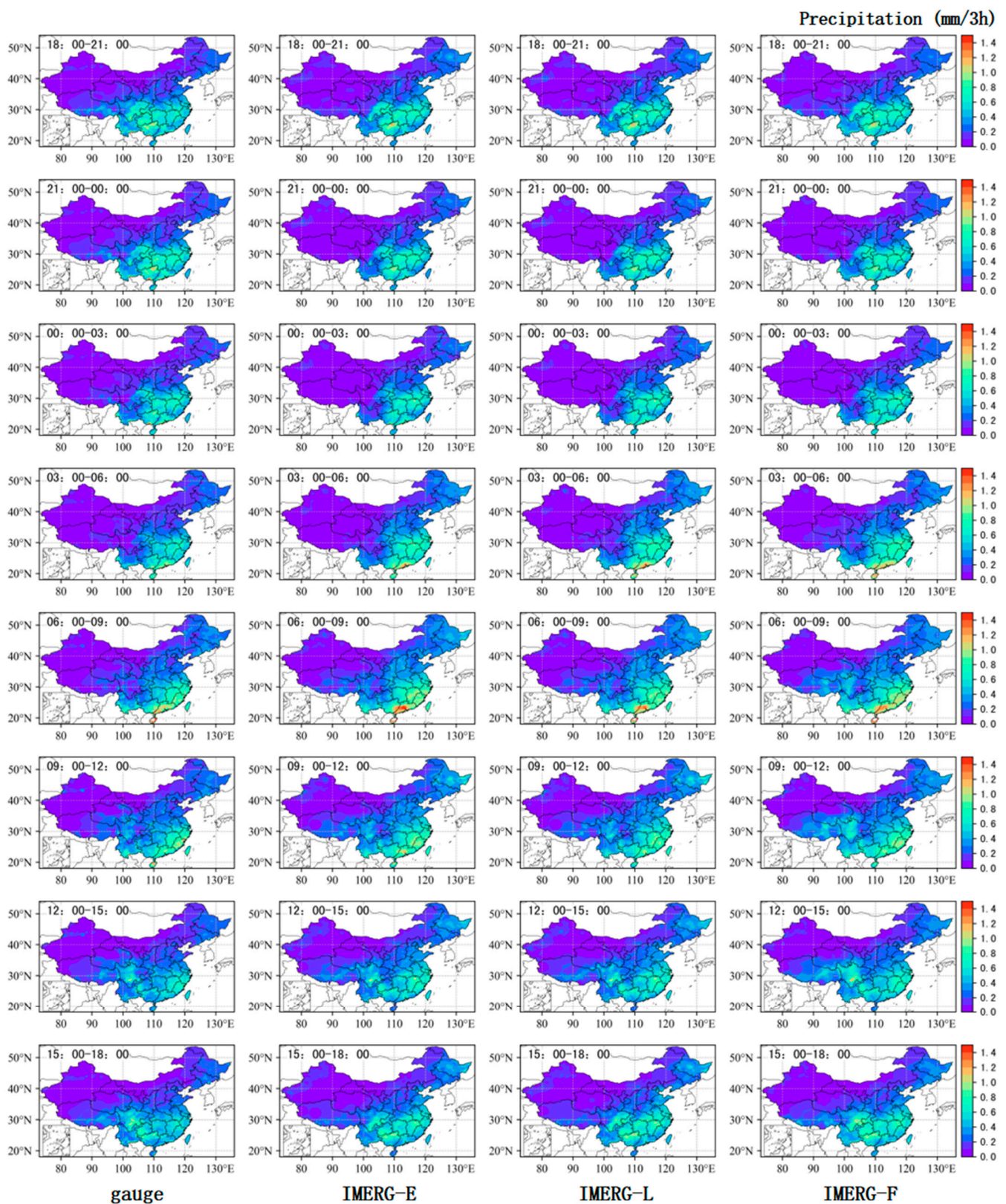


Figure 8. Spatial distribution of three-hourly average rainfall (UTC, coordinated universal time) estimated from ground stations and GPM satellite products from June 2014 to December 2020, with gauge, IMERG-E, IMERG-L, and IMERG-F displayed from left to right.

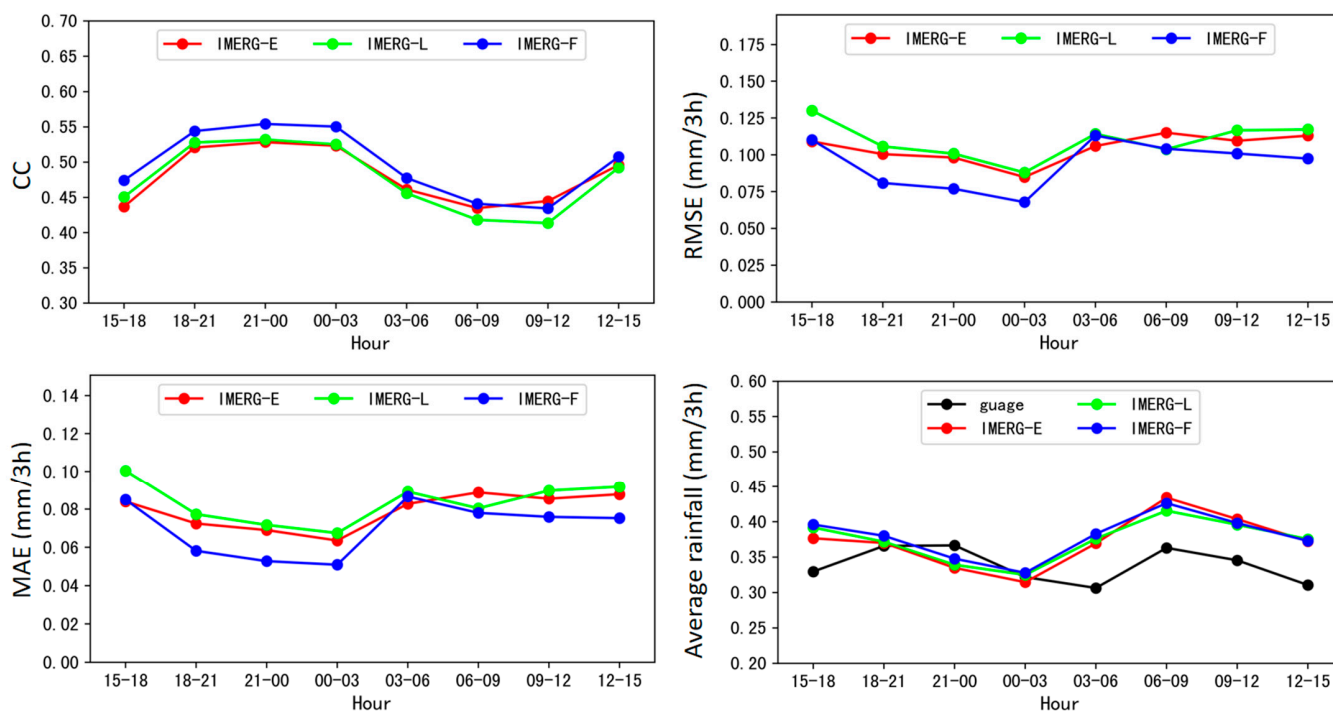


Figure 9. Temporal distribution of performance indices for GPM satellite products IMERG-E, IMERG-L, and IMERG-F on three-hourly basis (CC, RMSE, MAE, IMERG, and three-hourly average rainfall).

IMERG precipitation products perform better in light precipitation with higher correlation coefficients and lower RMSE and MAE. In contrast, GPM satellite products perform poorly in heavy precipitation with lower correlation coefficients and higher RMSE and MAE. Additionally, IMERG precipitation products perform the best during 00:00–03:00 with highest correlation coefficient and lowest RMSE/MAE.

Comparing the distribution of observed three-hourly precipitation and IMERG estimated precipitation, it is found that the IMERG precipitation products also exhibit a bimodal feature, but the corresponding time intervals of the peaks and valleys do not completely coincide with those of observed precipitation. Specifically, during the 06:00–09:00 period, the peak time of observed precipitation is more consistent with that of IMERG precipitation products, but the latter still shows overestimation. This may be due to the overestimation caused by the precipitation inversion process of the GPM satellite during daytime precipitation when it is more likely that errors occur in the inversion algorithm for small raindrops. Conversely, during the 21:00–00:00 h period, there is a significant difference between the peak time of actual precipitation and that of IMERG precipitation products, and the peak value of the GPM satellite product inversion is not obvious. This indicates that the tendency of GPM precipitation at night is poorer than that during the day, while its performance with respect to precipitation deviation is relatively better than during the day. This may be attributed to the higher atmospheric humidity and the larger raindrops during the night, reducing the inversion error of the GPM satellite since it lacks solar radiation.

In summary, based on the analysis of IMERG precipitation products at three-hourly timescale, it is found that their consistency with observed rainfall is generally weak, except for certain periods such as between 18:00–03:00 and 12:00–15:00, where the correlation coefficient ranges from 0.50 to 0.55. During periods of light precipitation, IMERG precipitation products show good performance with higher correlation coefficients and lower RMSE and MAE. Conversely, during periods of heavy precipitation, their performance is poor with low correlation coefficients and high RMSE and MAE. Among them, IMERG precipitation products perform the best during the peak and valley periods of hourly precipitation between 00:00–03:00 h, showing both higher correlation coefficients and lower errors. Al-

though IMERG precipitation products do not perform as expected in terms of the hourly precipitation, they exhibit good performance with higher correlation coefficients and lower errors during periods of light precipitation, indicating certain potential for future applications. Future research should further explore how to improve the performance of IMERG precipitation products at hourly timescale and find more effective evaluation criteria to provide more reliable data support for refined precipitation and hydrological forecasts.

3.4. Accuracy Analysis of Different Precipitation Intensities

From the comparison of sample proportions in different precipitation levels between ground observation and GPM satellite products (as shown in Figure 10), differences in sample proportions between ground observation and GPM satellite products are mainly reflected in no rain (<0.1 mm) and light rain levels. For no rain level, the sample proportion of ground observation is significantly higher than that of IMERG precipitation estimates; for light rain levels, the sample proportion of ground observation is significantly lower than that of IMERG precipitation products. This indicates that for no rain and light rain levels, there is a certain overestimation in IMERG precipitation products. By comparing the violin plots, it can be observed that there are obvious differences in the distribution of precipitation of gauge and IMERG products. Within the precipitation intensity range below 5 mm/d, the gauge exhibits a wider distribution of precipitation, indicating that the majority of precipitation is concentrated below 5 mm/d. In the 5–10 mm/d precipitation intensity range, the distribution of gauge narrows relative to IMERG, suggesting that IMERG has a higher proportion of precipitation within this range compared to gauge. Additionally, the quartiles of the violin plot for gauge are noticeably lower than those of IMERG, indicating that IMERG tends to overestimate precipitation below 10 mm/d. Among the IMERG products, the violin plot of IMERG-F consistently exhibits a narrower shape, indicating a more pronounced overestimation relative to the gauge. This may be related to various factors such as the performance of GPM satellite sensors, precipitation types, terrain influence, and retrieval algorithm and model errors, which need further analysis and research. For moderate and above precipitation intensities, the sample proportions of ground observation and GPM satellite products are similar, indicating that they are more consistent in the distribution of these precipitation levels.

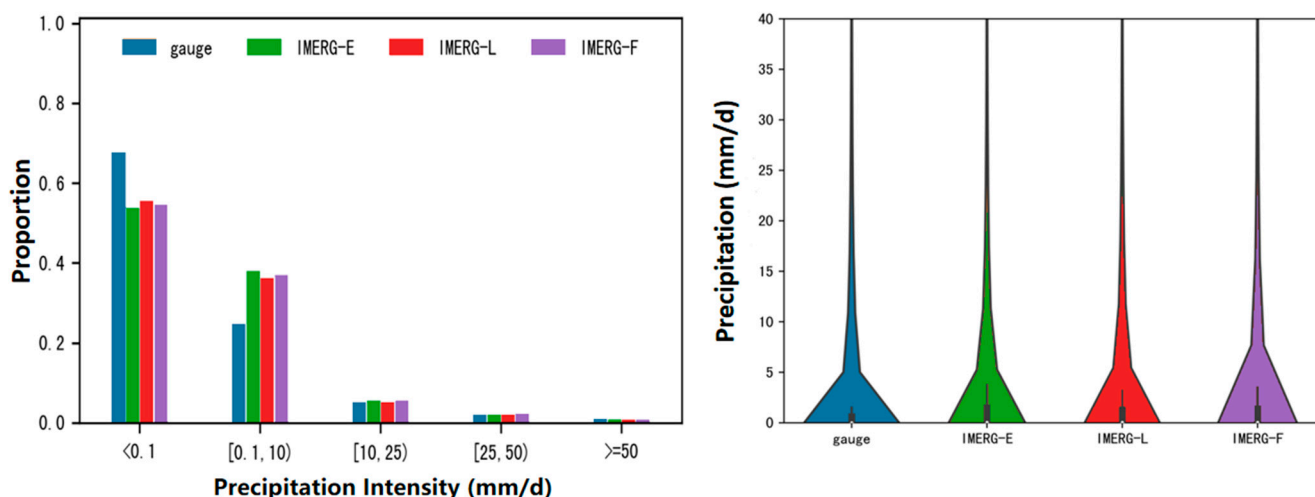


Figure 10. Comparison of sample proportions at different precipitation intensities for ground observation and GPM products, i.e., IMERG-E, IMERG-L, and IMERG-F, as well as the corresponding violin plot.

Figure 11 displays the detection capability of IMERG products at different precipitation intensity thresholds (no precipitation, light rain, moderate rain, heavy rain, and torrential rain and above). It can be seen that the POD index of GPM IMERG products

decreases with increasing precipitation intensity in heavy rain and below, and increases again in torrential rain and above. This increase may be due to the fact that precipitation levels above torrential rain was not subdivided. If precipitation levels above 50 mm are subdivided, the overall trend of the POD index will show a downward trend. Under different precipitation intensities, GPM satellite products show different POD, FAR, bias, and ETS performances. The POD index is highest in the no precipitation level, reaching 0.72 (IMERG-F), and lowest in the heavy rain level, only 0.27 (IMERG-E). The FAR index is significantly lower in the no precipitation level than in other precipitation intensity levels, and is less than 0.12 for all levels, with a minimum of 0.11 (IMERG-F); it increases with increasing precipitation intensity below heavy rain, and decreases again above torrential rain, which is similar to the trend of the POD index. The bias index shows that there is significant overreporting (bias > 1) in GPM precipitation products under light rain intensity, with bias indices around 1.5. For precipitation above moderate rain intensity, the bias index is close to 1, indicating that GPM satellite products are relatively accurate in estimating precipitation above moderate rain intensity. The ETS index shows that IMERG precipitation products perform similar between light and heavy rain intensities, with ETS values ranging from 0.15 to 0.18. In the absence of precipitation and in cases of torrential rain and above, ETS scores are relatively high, with no precipitation level having the highest score, ranging from 0.29 to 0.32.

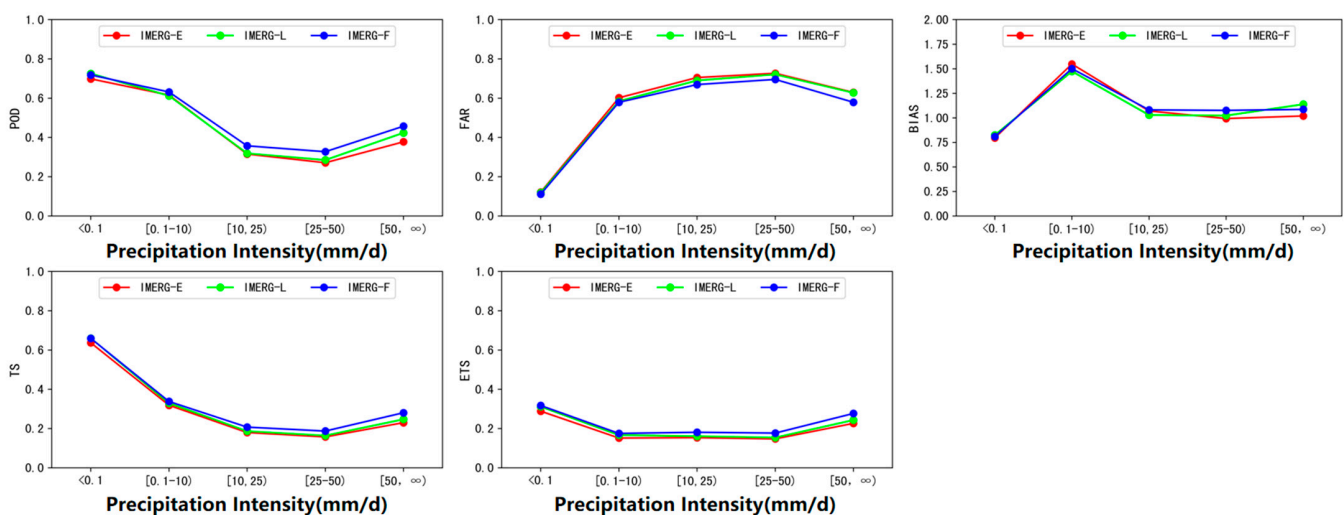


Figure 11. Temporal distribution of evaluation indices (POD, FAR, bias, TS, and ETS) for various precipitation intensity.

Overall, IMERG-F performs better than IMERG-L and IMERG-E. Performance in the absence of precipitation and under light rain intensity is better than that under moderate and above precipitation intensities. Based on the analysis of the detection capability and overall performance, valuable information can be provided for improving the accuracy of IMERG precipitation products under various precipitation intensities.

4. Conclusions

The purpose of this study is to evaluate the reliability of GPM satellite precipitation products in China. We evaluated the accuracy of GPM IMERG products at different spatial and temporal scales against ground observations.

(1) The performance of IMERG products at different spatial scales

GPM IMERG precipitation products perform better in the eastern and southern regions, while relatively poorer in the western and northern regions. Especially in the northwest region, there is a significant deviation in the performance of GPM precipitation products. These differences may be related to factors such as topography, climate, and gauge density

used in bias correction. In the western and northern regions, complex terrain may cause large variations in the spatial distribution of precipitation, thereby affecting the accuracy of GPM precipitation products. In addition, low gauge density in these areas may magnify errors in satellite products.

(2) The performance of IMERG products at different temporal scales

GPM satellite precipitation products perform best in summer and worst in winter. This may be because precipitation in China is more abundant in summer, making satellite detection relatively easier, while winter precipitation is less frequent and more complex in type and form, resulting in increased difficulty in satellite detection. In addition, changes in atmospheric water vapor content at different seasons may also affect the performance of satellite precipitation products.

(3) The performance of IMERG products at different precipitation intensities

GPM precipitation products perform well for light and no precipitation. However, their accuracy gradually decreases with increasing intensity due to the saturation tendency of satellite echoes.

Overall, this study evaluated the performance of GPM satellite precipitation products at different spatial and temporal scales for various precipitation intensities over China. This evaluation provides valuable information for improving the accuracy of GPM and other satellite precipitation products. It also presents a comprehensive perspective to understand the applicability of GPM satellite precipitation products in China, especially for those hydrological-modeling-based applications using the IMERG products. Therefore, future work could focus on improving the accuracy of real-time satellite precipitation data through the refinement of corrections for IMERG precipitation data. Additionally, it would be valuable to assess the applicability of these improved satellite precipitation data in hydrological modeling in China.

Author Contributions: Conceptualization, H.W., S.C. and X.P.; methodology, X.P.; software, X.P.; validation, X.P.; formal analysis, X.P.; investigation, X.P. and X.L.; resources, W.C., Z.H. and C.L.; data curation, X.P. and Z.H.; writing—original draft preparation, X.P.; writing—review and editing, H.W., N.N. and X.P.; visualization, X.P.; supervision, H.W., N.N. and S.C.; project administration, H.W.; funding acquisition, H.W. All authors have read and agreed to the published version of the manuscript.

Funding: This study was supported by the Key R&D Program of Guangxi (Guike AB21075008), the National Natural Science Foundation of China (grant numbers: 42088101, 42275019, and 41905101), and also partially supported by the Program for Guangdong Introducing Innovative and Entrepreneurial Teams (grant numbers: 2017ZT07X355 and 2020B1212060025) and Hainan R&D Program (grant numbers: CXFZ2022J074 and SCSF202203).

Data Availability Statement: The Integrated Multi-Satellite Retrievals for Global Precipitation Version 6 (IMERG V06) datasets used in this study can be downloaded from <https://gpm.nasa.gov/GPM> (accessed on 15 June 2022).

Conflicts of Interest: The authors declare no conflict of interest.

References

1. Hou, A.Y.; Kakar, R.K.; Neeck, S.; Azarbarzin, A.A.; Kummerow, C.D.; Kojima, M.; Oki, R.; Nakamura, K.; Iguchi, T. The global precipitation measurement mission. *Bull. Am. Meteorol. Soc.* **2013**, *95*, 701–722. [\[CrossRef\]](#)
2. Henderson-Sellers, A. The water cycle. In *Encyclopedia of Climate and Weather*; Schneider, S.H., Ed.; Oxford University Press: Oxford, UK, 1996; pp. 912–919.
3. Blacutt, L.A.; Herdies, D.L.; de Goncalves, L.G.; Vila, D.A.; Andrade, M. Precipitation comparison for the cfsr, merra, trmm3b42 and combined scheme datasets in bolivia. *Atmos. Res.* **2015**, *163*, 117–131. [\[CrossRef\]](#)
4. Yu, R.C.; Li, J.; Chen, H.M.; Yuan, W.H. Research progress on diurnal variation of precipitation in mainland China. *Acta Meteorol. Sin.* **2014**, *72*, 948–968.
5. Li, B. Development of weather radar technology in China and its challenges. *Adv. Meteorol. Sci. Technol.* **2022**, *12*, 37–46.
6. Mahmoud, M.T.; Al-Zahrani, M.A.; Sharif, H.O. Assessment of global precipitation measurement satellite products over Saudi Arabia. *J. Hydrol.* **2018**, *559*, 1–12. [\[CrossRef\]](#)

7. Duan, Z.; Liu, I.Z.; Tuo, Y.; Chiogna, G.; Disse, M. Evaluation of eight high spatial resolution gridded precipitation products in Adige Basin (Italy) at multiple temporal and spatial scales. *Sci. Total Environ.* **2016**, *573*, 1536–1553. [[CrossRef](#)]
8. Hu, Z.; Zhang, C.; Hu, Q.; Tian, H. Temperature changes in Central Asia from 1979 to 2011 based on multiple datasets. *J. Clim.* **2014**, *27*, 1143–1167. [[CrossRef](#)]
9. Gou, Y.; Ma, Y.; Chen, H.; Wen, Y. Radar-derived quantitative precipitation estimation in complex terrain over the eastern Tibetan Plateau. *Atmos. Res.* **2018**, *203*, 286–297. [[CrossRef](#)]
10. Alfieri, L.; Claps, P.; Laio, F. Time-dependent ZR relationships for estimating rainfall fields from radar measurements. *Nat. Hazards Earth Syst. Sci.* **2010**, *10*, 149–158. [[CrossRef](#)]
11. Lu, X.; Tang, G.; Wei, M.; Yang, L.; Zhang, Y. Evaluation of multi-satellite precipitation products in Xinjiang, China. *Int. J. Remote Sens.* **2018**, *39*, 7437–7462. [[CrossRef](#)]
12. Nanding, N.; Rico-Ramirez, M.A.; Han, D. Comparison of different radar-raingauge rainfall merging techniques. *J. Hydroinform.* **2015**, *17*, 422–445. [[CrossRef](#)]
13. Nanding, N.; Rico-Ramirez, M.A.; Han, D.; Wu, H.; Dai, D.; Zhang, J. Uncertainty assessment of radar-raingauge merged rainfall estimates in river discharge simulations. *J. Hydrol.* **2021**, *603*, 127093. [[CrossRef](#)]
14. Zhang, A.Q.; Fu, Y.F. Case study of precipitation structure detection using dual-frequency radar on GPM satellite. *Atmos. Sci.* **2018**, *42*, 33–51.
15. Chen, T.; Dong, L.; Luo, L.; Yang, S.N. Convective structure characteristics and its impact on heavy rainfall during Typhoon Lekima landfall. *Meteorology* **2021**, *47*, 1433–1443.
16. Giannaros, C.; Dafis, S.; Stefanidis, S.; Giannaros, T.M.; Koletsis, I.; Oikonomou, C. Hydrometeorological analysis of a flash flood event in an ungauged Mediterranean watershed under an operational forecasting and monitoring context. *Meteorol. Appl.* **2022**, *29*, e2079. [[CrossRef](#)]
17. Bezak, N.; Borrelli, P.; Panagos, P. Exploring the possible role of satellite-based rainfall data in estimating inter- and intra-annual global rainfall erosivity. *Hydrol. Earth Syst. Sci.* **2022**, *26*, 1907–1924. [[CrossRef](#)]
18. Sheffield, J.; Wood, E.F.; Pan, M.; Beck, H.; Coccia, G.; Serrat-Capdevila, A.; Verbist, K. Satellite remote sensing for water resources management: Potential for supporting sustainable development in data-poor regions. *Water Resour. Res.* **2018**, *54*, 9724–9758. [[CrossRef](#)]
19. Mahmoud, M.T.; Mohammed, S.A.; Hamouda, M.A.; Dal Maso, M.; Mohamed, M.M. Performance of the IMERG Precipitation Products over High-latitudes Region of Finland. *Remote Sens.* **2021**, *13*, 2073. [[CrossRef](#)]
20. Lu, N. Evaluation of IMERG Precipitation Products in the Southeast Coastal Urban Region of China. *Remote Sens.* **2022**, *14*, 4947. [[CrossRef](#)]
21. Dong, W.; Wang, G.; Guo, L.; Sun, J.; Sun, X. Evaluation of Three Gridded Precipitation Products in Characterizing Extreme Precipitation over the Hengduan Mountains Region in China. *Remote Sens.* **2022**, *14*, 4408. [[CrossRef](#)]
22. Yan, Y.; Wang, G.; Nanding, N.; Chen, W. Hydrological evaluation of satellite-based precipitation products in Hunan Province. *Remote Sens.* **2022**, *14*, 3127. [[CrossRef](#)]
23. Zhang, R.; Yong, B.; Zeng, S.K. Accuracy assessment of GPM satellite precipitation products over mainland China. *People's Yangtze River* **2021**, *52*, 50–59. [[CrossRef](#)]
24. Li, J.; Yong, B.; Wu, H. Error analysis of FY4A and GPM precipitation inversion products in mainland China (Online). *Remote Sens. Technol. Appl.* **2023**, 1–14. [[CrossRef](#)]
25. Ren, Y.J.; Yong, B.; Lu, D.K.; Chen, H.Q. Multi-scale accuracy assessment of IMERG satellite precipitation product over mainland China based on Global Precipitation Measurement mission multi-satellite precipitation analysis. *J. Lake Sci.* **2019**, *02*, 560–572.
26. Long, Y.P.; Chen, G.Y.; Ma, Q.M.; Chen, J. Ground validation of Fengyun-4A and Global Precipitation Measurement satellite observations over an alpine and canyon basin of the southeastern Tibetan Plateau. *J. Mt. Sci.* **2022**, *19*, 3568–3581. [[CrossRef](#)]
27. Sun, G.K.; Wei, Y.X.; Wang, G.S.; Shi, R.; Mo, C.X. Applicability analysis of GPM IMERG satellite precipitation data in Guangxi region. *People's Yangtze River* **2022**, *53*, 98–106. [[CrossRef](#)]
28. Li, X.H.; Sun, Y. Accuracy validation and error decomposition of satellite precipitation products in Sichuan-Chongqing region. *People's Yangtze River* **2022**, *53*, 97–103. [[CrossRef](#)]
29. Li, Y.N.; Huang, C.; Pang, G.W. Accuracy assessment of GSMaP and IMERG satellite precipitation products in Shaanxi region, China. *Arid Land Geogr.* **2022**, *45*, 80–90.
30. Wang, Z.T.; Li, S.B.; Zhang, Z.Y. Multi-scale accuracy evaluation of GPM near real-time precipitation product over the Qinghai-Tibet Plateau. *People's Yangtze River* **2021**, *43*, 43–49+116.
31. Qu, X.; Fu, Y.; Yuan, X.; Xie, X.; Bai, M. Applicability analysis of GPM-IMERG daily precipitation data in Inner Mongolia. *Torrential Rain Disasters* **2020**, *39*, 293–299. [[CrossRef](#)]
32. Zhang, H.L.; Xiao, L.S.; Chen, S.; Wu, N.G. Diurnal variation characteristics and assessment of precipitation during flood season in Guangdong based on GPM satellite. *J. Trop. Meteorol.* **2020**, *39*, 335–346. [[CrossRef](#)]
33. Chen, F.J.; Li, Y.X.; Gao, J.L.; Wang, Y.; Zhu, H.L. Verification of IMERG and TMPA precipitation products in summer over central and eastern China. *Meteorol. Mon.* **2019**, *12*, 1680–1690.
34. Wang, H.T.; Zhang, X.X.; Zhao, M.C.; Shu, W.M. Accuracy assessment of TMPA and IMERG satellite precipitation products in the Three Gorges region. *J. Yangtze River Sci. Res. Inst.* **2019**, *12*, 23–27.

35. Chen, F.; Li, X. Evaluation of IMERG and TRMM 3B43 Monthly Precipitation Products over Mainland China. *Remote Sens.* **2016**, *8*, 472. [[CrossRef](#)]
36. Tian, F.; Hou, S.; Yang, L.; Hu, H.; Hou, A. How does the evaluation of the GPM IMERG rainfall product depend on gauge density and rainfall intensity? *J. Hydrometeorol.* **2018**, *19*, 339–349. [[CrossRef](#)]
37. Tang, G.; Ma, Y.; Long, D.; Zhong, L.; Hong, Y. Evaluation of GPM Day-1 IMERG and TMPA Version-7 legacy products over Mainland China at multiple spatiotemporal scales. *J. Hydrol.* **2016**, *533*, 152–167. [[CrossRef](#)]
38. Kazamias, A.P.; Sapountzis, M.; Lagouvardos, K. Evaluation of GPM-IMERG rainfall estimates at multiple temporal and spatial scales over Greece. *Atmos. Res.* **2022**, *269*, 106014. [[CrossRef](#)]
39. Shi, L.J.; Feng, W.Y.; Lei, Y.; Wang, Z.M.; Zeng, Q. Accuracy evaluation of daily GPM precipitation product over Mainland China. *Meteorol. Mon.* **2022**, *48*, 1428–1438.
40. Xu, J.T. Precipitation Accuracy Evaluation and Fusion Correction Research of IMERG Precipitation Products in Mainland China. Ph.D. Thesis, Zhejiang University, Hangzhou, China, 2020. [[CrossRef](#)]
41. Pan, Y.; Gu, J.X.; Shi, C.X.; Wang, Z. Evaluation and fusion optimization of multi-source data products for winter precipitation in northern China. *Acta Meteorol. Sin.* **2022**, *80*, 953–966.
42. Jin, X.L.; Shao, H.; Qiu, Y.; Du, H.Y. Research on calibration methods of TRMM satellite precipitation data in Tianshan mountainous area. *Meteorol. Mon.* **2018**, *44*, 882–891.
43. Nanding, N.; Wu, H.; Tao, J.; Maggioni, V.; Beck, H.E.; Zhou, N.; Huang, M.; Huang, Z. Assessment of Precipitation Error Propagation in Discharge Simulations over the Contiguous United States. *J. Hydrometeorol.* **2021**, *22*, 1987–2008. [[CrossRef](#)]

Disclaimer/Publisher’s Note: The statements, opinions and data contained in all publications are solely those of the individual author(s) and contributor(s) and not of MDPI and/or the editor(s). MDPI and/or the editor(s) disclaim responsibility for any injury to people or property resulting from any ideas, methods, instructions or products referred to in the content.